11th International Symposium on Magnetic Bearings
August 26-29, Nara, Japan

PASSIVE ATTRACTION REDUCTION FOR LINEAR PERMANENT MAGNET ACTUATORS

J.J.H. Paulides
Dept. of Electrical Eng., Eindhoven University of Technology, The Netherlands
j.j.h.paulides@tue.nl

J.L.G. Janssen
Dept. of Electrical Eng., Eindhoven University of Technology, The Netherlands
j.l.g.janssen@tue.nl

E. Lomonova
Dept. of Electrical Eng., Eindhoven University of Technology, The Netherlands
e.lomonova@tue.nl

ABSTRACT

With the ever advancement and increased force density of slotted brushless linear permanent magnet (PM) actuators the attraction forces become more dominating. Where in the early years this attraction force was advantageous it now becomes a problem due to reduced bearing lifetime.

INTRODUCTION

The increasingly widespread industrial applications of permanent magnet (PM) linear actuators in various semiconductor processes, precision metrology, and miniature system assembly are self-evident testimonies of the effectiveness of these PM actuators in addressing the high requirements associated with these application areas. As such, today's brushless PM linear actuators are evermore implemented, since they incorporate a high power and torque density and provide the most efficient motor technology available to the industry [1, 2]. Further, high accuracies at rapid movements can be achieved, which results in consistent and repeatable machine performance, e.g in various areas of manufacturing automation. In these applications, robot manipulators for the pick-and-place and assembly tasks require both accurate positioning and high speed motion. As such, considering the available pick-and-place machine concepts, numerous machine concepts could be used to perform the pick-and-place action, however, this paper focuses on a robot with static PCB board and multiple moving robots placing multiple components [3]. The industry has realized that this concept can only be significantly enhanced by applying direct-drive PM actuator for the long-stroke of the pick-and-place robot. As such a demonstrator robot has been built using the direct-drive technology (Fig.1).

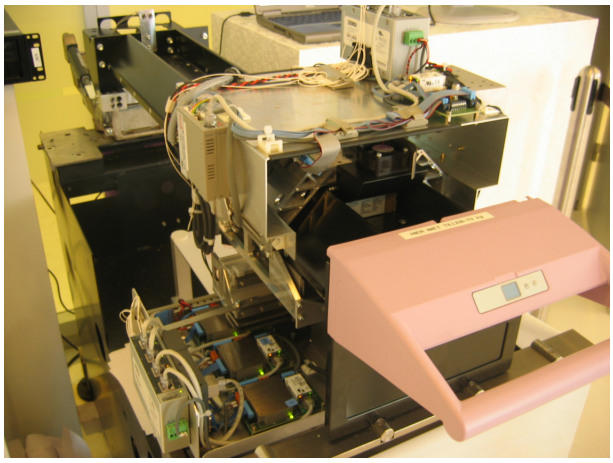

FIGURE 1: Industrially developed concept of a single unit pick-and-place robot.

In these direct-drive iron cored brushless permanent magnet (PM) linear machines used in this application, silicon laminations are used to maximize the thrust forces. However, these iron cores also introduce both cogging and attraction forces between the iron mover and the PM's. Most commercial brushless PM linear machines are designed to minimize these forces to allow them to be used in high precision constant velocity applications. However, in this respect the attraction force is, in general, less considered in the design of PM actuators although that [4] reports a double sided moving magnet linear actuator that has a reduced attraction force. In most linear applications having some attraction force can be advantageous, e.g. to preload the air of mechanical bearings. However, if large attraction forces are apparent, this will impede on the bearing lifetime. Therefore, some passive components can be used to counter-act these forces, as shown in Figure 2.

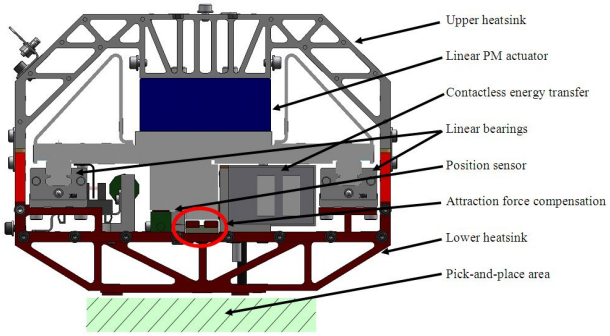

FIGURE 2: Cross-section of the contactless pick-and-place robot.

MOVING COIL LINEAR ACTUATOR

In many high precision applications (Fig. 1), the moving-coil linear PM actuator is applied due to its commercial maturity and relative simple sensor technology, albeit that the attraction force is apparent in both moving-magnet and -coil linear PM actuators. Numerous active or passive solutions can be investigated to reduce this attraction force, where passive systems have the positive peculiarity that they require very low energy consumption and an unlimited track length. One possible solution for such a passive magnetic levitation system is to use passive attraction compensation PMs, as illustrated in Figure 3.

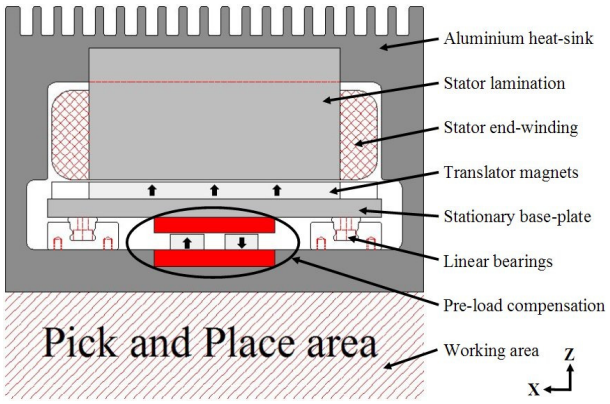

FIGURE 3: Schematic representation of Figure 2, the y-axis actuator of a pick-and-place machine.

This has the advantage that little PM material is required, hence only small costs, however has the disadvantage that a construction is needed to enable the PM to be placed so that the attraction can be utilized, although that in e.g. a pick-and-place application this construction could be used to mount the placement actuators. Another possible solution for the magnetic levitation system is a passive repulsive one on top of the linear actuator, which is based on two magnetic guides, with PMs. These magnetic guides provide the lifting force by employing the repulsive force generated by the interaction between a long magnet, mounted along the way and a short permanent magnet mounted on the moving coil assembly. This configuration has the advantage that it does not require a separate construction, however increases the width of the pick-and-place robot, which is not desirable in a machine which employs multiple robots [3].

BEARING LIFETIME

The linear bearings in this moving-coil linear actuator system could be taken very large, however this would occupy a large proportion of the available space, hence it would be beneficial to minimize the linear bearing by providing a passive attraction force that counteracts the gravitational and attraction force. This lighter linear bearing system enables more rapid movements and the costs are considerably lower, whilst its lifespan will be longer [5]. The selected smaller linear bearings are a commercial rail guide assembly (Speedi-Roll size 25), where the length of travel is 1500mm and the stroke frequency is 5Hz. This linear guide system provides rigidity and torque resistance and consists of a guide rail and a carriage with three rollers. The rail is composed of a drawn and anodized aluminum body with hardened steel angle raceways fitted on each side. The aluminum base plate of the carriage, which is also anodized, houses the factory-fitted rollers. The load, centrally applied on these linear bearings, is constant in magnitude and direction (see Figures 2 and 3). The static load rating of this bearing system is 1400 N and is expected to be moved smoothly without any shocks. The life of the linear table, in km and hours of operation, as well as the static safety factor of the system are required. The lifetime in modified nominal working hours, L_{life}, is calculated by [6]:

$$L_{life} = \frac{50000}{s\, n_f\, 60}\left(\frac{C\, f_l}{P\, f_d}\right)^3, \qquad (1)$$

where s is the stroke in m, n_f is the frequency of the stroke in minutes, C is a linear bearing constant, $f_l = 0.8$ (for only normal force) and $f_d = 1.0$ (for smooth load conditions). For a commercial linear PM actuator the attraction force combined with an additional pay-load mass of 7.5 kg a total attraction force by the moving coils of approximately 975 N exists (TL6 www.tecnotion.com). Assuming the use of 3 linear bearing units, the dynamic load per bearing is 325 N, which results in a 1.5 year bearing lifetime. This, for example, requires an attraction force compensation of 575 N for a sought after bearing lifetime of approximately 10 years. The next section presents passive magnetic solutions to provide for this, mainly, vertical force compensation.

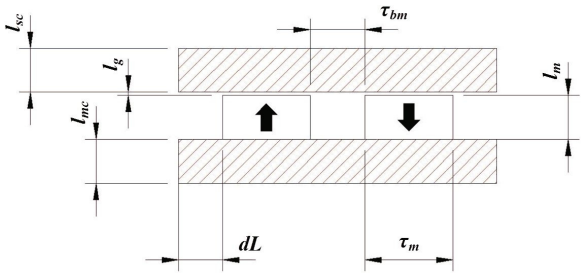

FIGURE 4: Schematic representation of the y-axis actuator of a pick-and-place machine.

2D ATTRACTION FORCE CALCULATION

The attraction force can be calculated using the Maxwell stress tensor. This tensor has to be integrated over a closed surface in air around the magnet array to calculate the total attraction force on the permanent magnets. The force on the magnets is obtained by:

$$F_{att} = \oiint \frac{1}{\mu_0} \begin{bmatrix} \frac{1}{2}\left(B_x^2 - B_y^2 - B_z^2\right) & B_x B_y & B_x B_z \\ B_x B_y & \frac{1}{2}\left(B_x^2 - B_y^2 - B_z^2\right) & B_y B_z \\ B_x B_z & B_y B_z & \frac{1}{2}\left(B_x^2 - B_y^2 - B_z^2\right) \end{bmatrix} \cdot n \, \mathrm{d}S \tag{2}$$

where B_x, B_y and B_z are the flux densities, n is the unity vector perpendicular to the surface element dS. In this analysis the B_x and B_y are considered to be zero, since, neglecting fringing, all the flux flows along the z-axis (Figure 3). The B_z component can also be considered as the flux density within the middle of the airgap, B_g, which simplifies (3) to:

$$F_{att} = \frac{B_g^2 A_m}{2\mu_0}, \tag{3}$$

where A_m is the total area of both permanent magnets, μ_0 is the relative permeability of air and B_g is the flux density can be expressed by neglecting saturation or leakage effects by:

$$B_g = \frac{B_r}{1 + \mu_r \frac{l_g A_m}{l_m A_g}}. \tag{4}$$

In this l_g and l_m are the airgap and magnet length, A_g and A_m are the airgap and magnet area. Using a high grade NdFeB magnet the remanent flux density, B_r, is 1.23 T and the recoil permeability, μ_r, is 1.05.

TABLE I
INITIAL GEOMETRY DIMENSIONS

Stationary core length	l_{sc}	5.0 mm
Airgap length	l_g	0.3 mm
Magnet length	l_m	4.0 mm
Moving core length	l_{mc}	5.0 mm
Extra width	dL	1.0 mm
Magnet pitch	τ_m	8.0 mm
Between magnet pitch	τ_{bm}	0.1 mm

Applying the dimensions of Table 1 to the geometry of Figure 4, results in an attraction force of 8277 N/m, hence using an axial length of 70 mm a 579 N attraction force. As mentioned this neglects 3D effect in the flux calculation, hence a more comprehensive model will be introduced in the next section to verify the results of using the 2D Maxwell stress tensor to calculate the attraction force.

3D ATTRACTION FORCE CALCULATION

Considering the topology of two permanent magnets between iron bodies, normally the Finite Element Method (FEM) would be used to calculate the attraction force between the bodies, however, this method is rather time consuming. Therefore, an analytical approach is considered.

The 3D analytical surface charge method [7], provides fast solving analytical expressions of the interaction force between permanent magnets in free space. More specifically, these analytical solutions are not mesh based, and therefore exhibit their high accuracy especially at large magnetic field gradients (e.g. the magnet edges). This makes them especially suitable for applications having small air gaps.

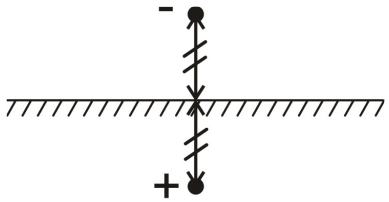

FIGURE 5: Schematic example of the 2D imaging technique, showing the charged particle (-), and its image in the metal (+).

The analytical charge model is based on the assumption that there are no materials present that influence the magnetic field, where the pre-load compensator incorporates significant volumes of flux-focusing material.

In the analytical mode, these high-permeable surfaces are dealt with using the charge imaging method. This method is based on the equality between the field due to a magnetically charged particle placed above an infinitely permeable half space and the field as if an oppositely charged particle would be placed equidistant below the surface. This is schematically shown in Fig. 5.

In [8] it is shown that the 2D field of a charged particle placed between two infinitely large and infinitely permeable half planes is equal to the field of an infinite array of images of this particle, mirrored in the surfaces of the half planes. Since the charge model expresses the permanent magnets as charges, the imaging technique is applied to model permanent magnets between iron volumes, although in 3D instead of the 2D described in [8]. Here, it is assumed that the iron volumes are infinitely permeable and infinitely large. The result of such imaging is schematically shown in Fig. 6. Although the number of images should be infinitely high for exact results, it has been found that applying 5 consecutive images in each half plane are sufficient to obtain accurate values for the attraction force. In total this gives 11 permanent magnet images of each PM along the vertical axis, all having the same dimensions as the original magnet. The sign change occurring for each image causes the magnetization pattern shown in Fig. 6b.

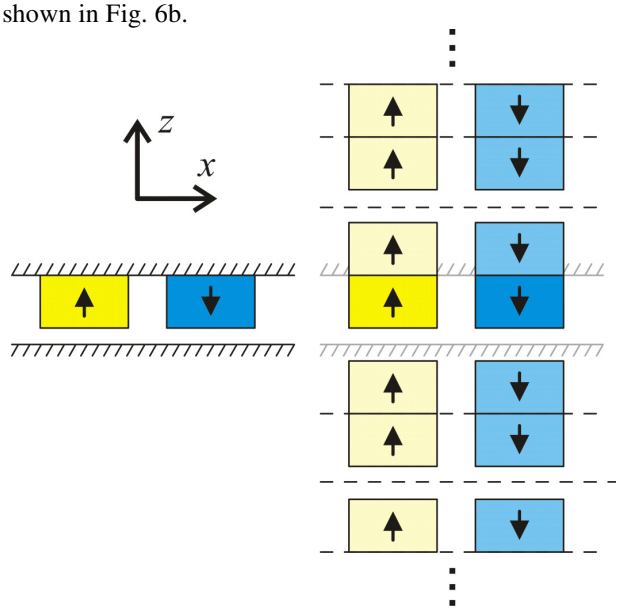

FIGURE 6: Schematic representation (a) 2 PMs between infinitely permeable half spaces and (b) the equivalent array of images in air.

Applying the dimensions of Table I, the obtained 3D analytical interaction attraction force equals 487N, which is well below the attraction force obtained from the 2D analytical model. Hence, a longer axial length is selected , being 83 mm, which provides an analytical force of 578 N. This difference in force between 2D and 3D analytical is caused by fringing, which is not incorporated in the 2D analytical model. Further, the analytical model does not consider saturation, hence a further numerical analysis is necessary to determine the back-iron thicknesses.

2D FINITE ELEMENT ANALYSIS

A 2D finite element analysis is used to incorporate the saturation effect, since it is more time efficient than the 3D analysis. In this analysis the materials used are the same as mentioned before, however additionally a non-linear mild-steel BH characteristic is implemented for the back-irons. Applying the dimensions of Table 1 with a large back-iron of 10 mm to the geometry of Figure 1, results in an attraction force of 7000 N/m, hence using an axial length of 82 mm provides attraction force of 575 N respectively.

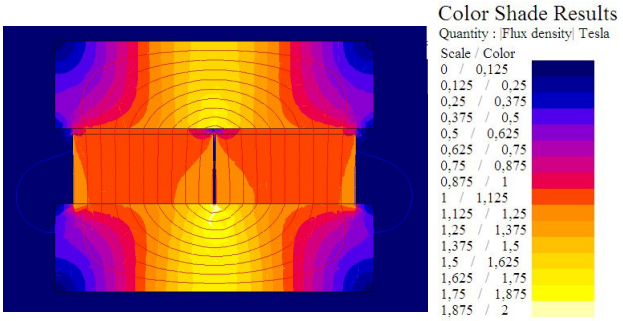

FIGURE 7: Equipotential contours and flux density for the passive attraction force with the initial dimensions of Table 1.

However, this back-iron length is not realistic and therefore the dimensions of Table 1 are used (Fig. 7), which decreases the attraction force to 6900 N/m, hence an axial length of 83 mm is required to attain the 573 N attraction force, which is equivalent to the axial length from the 3D analytical model.

To improve the model of Figure 1, the influence of the magnet length on the attraction force is investigated, as shown in Figure 8. This Figure shows that increasing the magnet length enhances the attraction force albeit at a diminishing rate. For example, a magnet length of 1.5 mm instead of 4.0 mm (62.5% reduction), only reduces the attraction force by 88 N (i.e. 578 N to 490 N or 15%). The corresponding total moving mass reduction is respectively 27.0 gr (or 31%), i.e. a 1.5 and 4.0 mm magnet length have a mass of respectively 60.5 and 87.5 gr (magnet and steel density respectively 7500 kg/m3 and 7600 kg/m3).

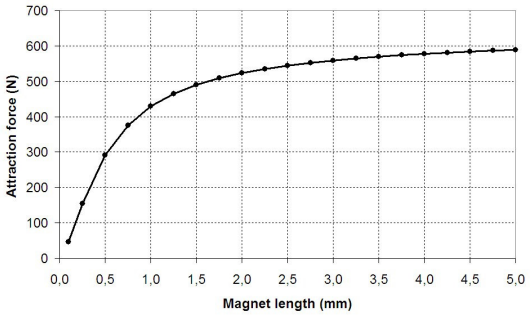

FIGURE 8: Variation of magnet length versus attraction force for the dimensions of Table 1.

It seems likely that some force improvement could be obtained when increasing the space in between magnet pitch, since it will reduce the magnet flux leakage. This was investigated, and increasing this to 1.0 mm increases the force by 1% (for lm = 1.5 mm), however this is not implemented, mainly, since manufacturing becomes a more dominant consideration, i.e. attached magnets could be more easily placed than separated magnets.

Further, the back-iron thickness should be varied to investigate its influence on the force, as shown in Fig. 4. This Figure shows that a back-iron thickness of 5.0 mm is a good compromise to maximize the force from an extended back-iron thickness.

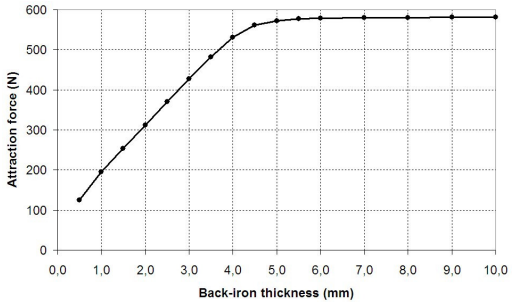

FIGURE 9: Variation of magnet length versus attraction force for the dimensions of Table 1.

Indeed a clear dependency of the back-iron thickness and the width of the magnet is apparent, hence a more comprehensive analysis is undertaken (Fig. 10) to illustrate the influence of both the back-iron thickness and magnet width on the attraction force. Clearly a very non-linear behavior becomes apparent when the back-iron saturates, which reduces the attraction force. This also influences the maximum achievable force for various magnet pitches, which shows the same linear characteristic as would be determined by the analytical method as discussed in the previous sections.

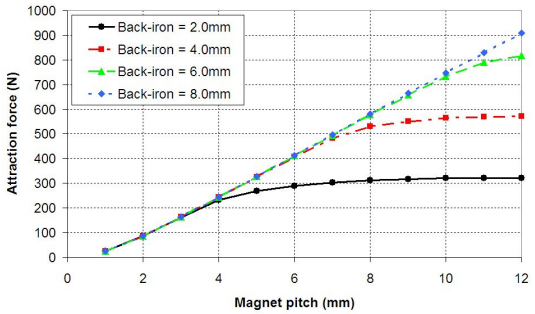

FIGURE 10: Variation of magnet pitch versus attraction force for various back-iron thicknesses.

Finally, it is also interesting to investigate the relationship between the mass and the magnet length, hence an extended analysis is undertaken to investigate this dependency. In this analysis all the remaining dimension are fixed to the values summarized in Table 1. Figure 11 shows the magnet length versus axial length and the magnet length versus the magnet mass for an attraction force of 575 N. This excludes the back-iron, which would only slightly amplify the values within this figure. Further, the magnet mass is arguably the most important characteristic, since it directly translates into costs of the compensator.

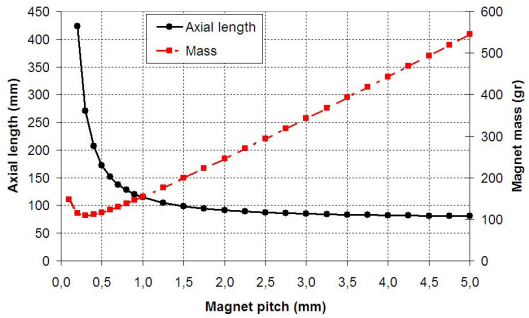

FIGURE 11: Variation of magnet length versus axial length and magnet length versus mass for an attraction force of 575 N.

Figure 11 clearly shows that, from a mass point-of-view, a very small magnet thickness is favored, however this at an extended stroke, e.g. an axial length and magnet length of 270 mm and 0.3 mm respectively. This, of course, does not present a practical solution, since the magnet is very small and the axial length is too large. In the pick-and-place application, the axial length is determined to be a maximum of around 90 mm and therefore a magnet length of 2.0 mm is selected for the compensation of the 575 N. The final dimensions have been summarized in Table 2, where the next section will

investigate these final dimensions using the 3D finite element analysis for verification.

TABLE II
INITIAL GEOMETRY DIMENSIONS

Stationary core length	l_{sc}	5.0 mm
Airgap length	l_g	0.3 mm
Magnet length	l_m	2.0 mm
Moving core length	l_{mc}	5.0 mm
Extra width	dL	1.0 mm
Magnet pitch	τ_m	8.0 mm
Between magnet pitch	τ_{bm}	0.1 mm
Axial length	τ_{bm}	93 mm

3D FINITE ELEMENT ANALYSIS

The objective of this final finite element study is to determine the force of the passive attraction and gravity permanent magnet compensator. The 2D model has been useful for determining the various influences of the variables in the 2D environment, where the effects of steel grade selection and 2D fringe effects are accounted. To complete the study also the 3D fringing effects are accounted for by a three-dimensional (3-D) finite element model, i.e. the 2D and 3D analysis provided an attraction force of 565 N and 559 N respectively.

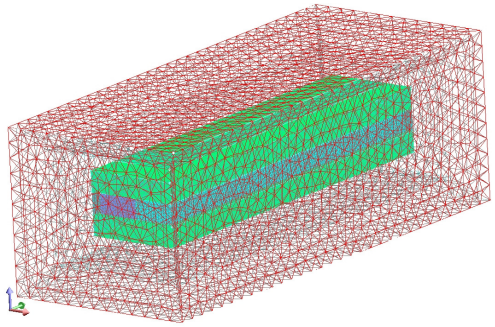

FIGURE 12: 3D finite element mesh for the dimensions of Table 2 (2550000 volume elements).

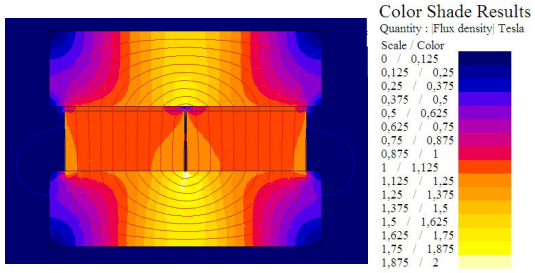

FIGURE 7: Equipotential contours and flux density for the compensator with the dimensions of Table 2.

PRACTICAL IMPLEMENTATION

Besides the concept application presented in the introduction also these attraction and gravity force compensators [5] are used in the H-bridge linear motor configuration (Fig. 13). In this Figure the passive compensator is encircled. As such, Fig. 14 shows the zoomed picture of the single DoF passive gravity compensator implemented in this machine. The same approach was used to calculate the force as was presented in this paper, where a very good agreement was apparent between the measurements and the finite element analysis.

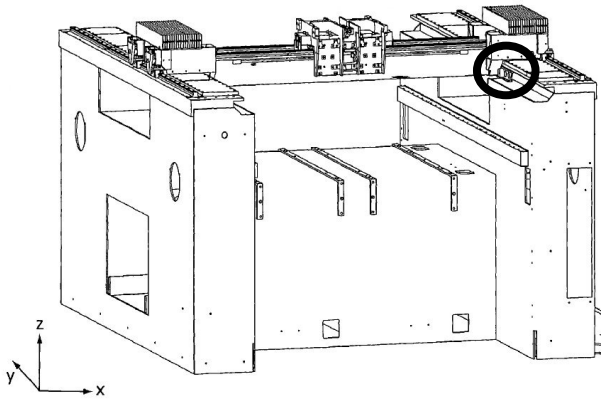

FIGURE 13: H-bridge pick-and-place machine topology.

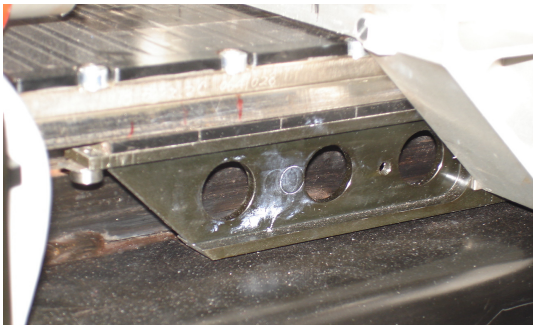

FIGURE 14: Practically applied passive attraction and gravity force compensator.

CONCLUSIONS

In order to extend the bearing lifetime a passive attraction and gravity permanent magnet compensator is selected. This configuration incorporates high strength rare earth PMs and a low cost commercial soft-magnetic material. The influence of this device on the bearing life has been investigated and various techniques for calculating the permanent magnet attraction force have been presented.

The relative dimensions have been optimized both by applying analytical equations as by implementing a finite element model. The influences of the main variables have

been presented, where a topology having a small magnet volume has been found and verified using 3D FEM.

To conclude, when moving a permanent magnet at considerable speed passes solid soft magnetic material, eddy-currents appear that results in a damping force. These losses have been identified, however are completely negligible since hardly any eddy-currents occur in the passive attraction and gravity permanent magnet compensator.

ACKNOWLEDGEMENT

The authors would like to acknowledge SenterNovem (Dutch Agency of Ministry of Economical Affairs) and Assembléon, which are all situated in the Netherlands, for their sponsorship.

REFERENCES

[1] D.L. Trumper, Kim Won-Jong and M.E. Williams, "Design and analysis framework for linear permanent-magnet machines", IEEE Trans. on Ind. Appl., Vol. 32, Issue 2, pp. 371-379, 1996.

[2] P. Heijmans, "LiMMS motor module", Philips report CTB595-95-4020, pp. 1-42, 1995.

[3] P.A.H. Goede, P.P.H. Verstegen, J.M.M. van Gastel, "Design of a shuttle used in an innovative pick and place machine concept," Proc. IEEE Int. Symp. on Ass. and Man., July 22-25, pp. 135-140, 2007.

[4] F. Profumo, A. Tenconi, G. Gianolio, "Design and realization of a PM linear Synchronous Motor with a very High Thrust/Normal Force ratio", IEEE Trans. on Ind. Appl., Vol. 3, pp. 1984-1988, 2001.

[5] J.H.A. van de Rijdt, "A displacement device as well as a component placement device", patent EP1895830A1, Assembléon Veldhoven, 2007.

[6] "Speedi-roll", www.linearmotion.skf.com

[7] J.P. Yonnet and G. Akoun, "3D analytical calculation of the forces exerted between two cuboidal magnets," IEEE Trans. Magn., vol. 20, no. 5, pp. 1962-1964, 1984.

[8] B. Hague, The principles of electromagnetism applied to electrical machines, New york: Dover Publications, 1962.